Sun, Q. D. *et al.* (2014). *Géotechnique* **64**, No. 9, 746–751 [http://dx.doi.org/10.1680/geot.14.T.015]

TECHNICAL NOTE

Effect of cyclic loading frequency on the permanent deformation and degradation of railway ballast

Q. D. SUN*, B. INDRARATNA† and S. NIMBALKAR†

A series of large-scale cyclic triaxial tests were conducted on latite basalt aggregates (ballast) to investigate how the frequency f affects the permanent deformation and degradation of railway ballast. During testing the frequency was varied from 5 Hz to 60 Hz to simulate a range of train speeds from about 40 km/h to 400 km/h. Three categories of permanent deformation mechanisms were observed in response to the applied cyclic loads, namely, the inception of plastic shakedown ($f \leqslant 20$ Hz), then plastic shakedown and ratcheting (30 Hz $\leqslant f \leqslant$ 50 Hz), followed by plastic collapse at higher frequencies ($f \geqslant 60$ Hz). The permanent strain of ballast and particle breakage increased with the frequency and number of load cycles. A cyclic strain ratio was introduced to capture the effect of frequency on the permanent axial and volumetric strains, respectively. An empirical equation was formulated to represent this relationship for latite basalt, and a critical train speed was identified. A good correlation was obtained between particle breakage and volumetric strain under cyclic loading.

KEYWORDS: deformation; failure; gravels; particle crushing/crushability; repeated loading; vibration

INTRODUCTION

There is an ongoing demand for better efficiency in rail transport, particularly increased freight capacity and greater speeds. Increased axle loads and the speed of trains increase the rate of ballast degradation that is characterised by unacceptable track deformation and the lateral spread of ballast, which leads to more frequent maintenance. In the past, cyclic triaxial tests have been conducted to characterise the permanent deformation of ballast (Suiker & de Borst, 2003; Lackenby *et al.*, 2007). Suiker & de Borst (2003) divided the stress domain (in q–p' space) of ballast under cyclic loading into four different response regimes: (*a*) shakedown, (*b*) cyclic densification, (*c*) frictional failure and (*d*) tensile failure. Cyclic triaxial data on ballast from Lackenby *et al.* (2007) are replotted in Fig. 1 to highlight the existence of at least four regimes of permanent deformation response based on the applied stress ratio ($q_{max,cyc}/p'$). These regimes are: (*a*) the zone of elastic shakedown exhibited by no plastic strain accumulation, (*b*) the zone of plastic shakedown characterised by a steady-state response with a small accumulation of plastic strain, (*c*) a ratcheting zone that shows a constant accumulation of plastic strain (Alonso-Marroquín *et al.*, 2004) and (*d*) a plastic collapse zone where the plastic strains accumulate rapidly and failure occurs in a relatively short time (Sloan *et al.*, 2008).

The influence of load frequency (f) on the accumulated plastic strain of granular material was negligible in those studies that simulate a low frequency range, that is $f \leqslant 10$ Hz (Youd, 1972; Wichtmann *et al.*, 2005; Karg & Haegeman, 2009). However, settlement was influenced significantly under high train speeds (Eisenmann *et al.*, 1994; Luo *et al.*, 1996; Kempfert & Hu, 1999; Banimahd *et al.*, 2013). On the basis of the finite-element analysis, Luo *et al.* (1996) showed that three distinct regimes of ballast settlement exist under different train speeds V (i.e. a low-speed region with an insignificant displacement, $V < 180$ km/h, an intermediate speed region with rapidly increasing displacement, 180 km/h $\leqslant V \leqslant$ 300 km/h, and a high-speed region with an attenuated increase in displacement, $V > 300$ km/h). Kempfert & Hu (1999) and Indraratna *et al.* (2014a) carried out in-situ measurements of dynamic forces induced by train speeds and reported that the stresses increased significantly with the train speeds. Indraratna *et al.* (2010a) applied different deviator stresses $q_{max,cyc}$ corresponding to the selected frequencies f; therefore, proper evaluation of the individual effects of $q_{max,cyc}$ and f was not possible. Hence, in the current paper, different frequencies were applied at a constant value of $q_{max,cyc}$ to simulate the effect of varying

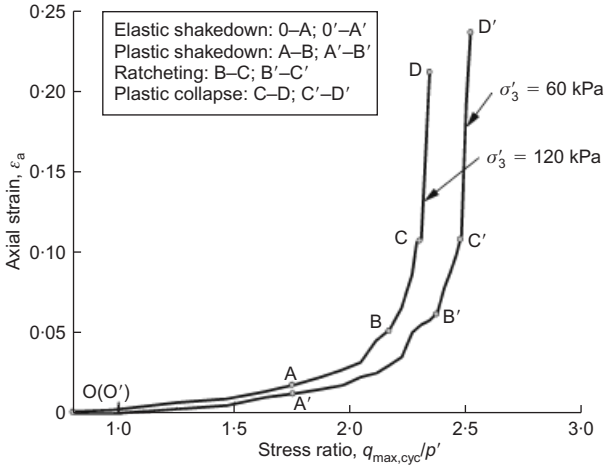

Fig. 1. Axial strain plotted against stress ratio (data sourced from Lackenby *et al.*, 2007)

Manuscript received 3 May 2014; revised manuscript accepted 12 August 2014. Published online ahead of print 12 September 2014. Discussion on this paper closes on 1 February 2015, for further details see p. ii.

* University of Wollongong, Wollongong, NSW, Australia.
† Centre for Geomechanics and Railway Engineering; ARC Centre of Excellence for Geotechnical Science and Engineering; University of Wollongong, Wollongong, NSW, Australia.

train speeds on the deformation and degradation of ballasted track.

LABORATORY INVESTIGATION

A large-scale triaxial apparatus (Indraratna *et al.*, 1998) was used to conduct isotropically consolidated, drained tests on ballast. The specimens (diameter = 300 mm, height = 600 mm) were prepared with preferred gradation and initial porosity ($d_{max} = 53$ mm, $d_{min} = 16$ mm, $d_{50} = 39{\cdot}5$ mm, $C_u = 1{\cdot}53$, $e_0 = 0{\cdot}76$). For more details on physical properties of the ballast, refer to Indraratna *et al.* (2014b). Each specimen was compacted to an initial density of 1530 kg/m^3 to simulate field densities for heavy haul tracks. Prior to testing, the specimen was saturated until a Skempton's B value of 0·97–0·98 was achieved. The lateral confinement provided by the sleepers, shoulder and crib ballast was mainly in the vicinity of 30 kPa (Indraratna *et al.*, 2010b), so a confining pressure of 30 kPa was applied. The cyclic deviator stress $q_{max,cyc}$ of 230 kPa represents 25 t axle load, and $q_{min,cyc}$ of 45 kPa represents in-situ stresses in the unloaded track (Lackenby *et al.*, 2007). The frequency is expressed as $f = V/L$, where V is train speed and L is the characteristic length between axles. Considering L of 2·02 m, frequency f is obtained as $0{\cdot}138\,V$ (Indraratna *et al.*, 2014c). The frequency f varied from 5 Hz to 60 Hz and resembles a range of train speeds from about 40 km/h to 400 km/h, respectively. Loading ceased after 500 000 cycles or when the vertical deformation almost reached the actuator displacement limit (at 30% axial strain). Before and after loading, the specimens were sieved to determine the extent of breakage using the ballast breakage index (BBI) (Indraratna *et al.*, 2005). Details of the experimental programme are given in Table 1.

EXPERIMENTAL RESULTS AND DISCUSSION

Permanent deformation behaviour

As described in the introduction, different zones of deformation for ballast that correspond to the increased magnitudes of cyclic load have already been described (Suiker & de Borst, 2003), but three ranges of deformation mechanisms occurred in this study as the frequency increased (i.e. 5 Hz $\leqslant f \leqslant$ 60 Hz) while the load magnitude was kept constant (i.e. $q_{max,cyc} = 230$ kPa), as described below

Range I: plastic shakedown (5 Hz $\leqslant f \leqslant$ 20 Hz). Figure 2(a) shows that when cyclic loads were applied, the axial strain ε_a developed rapidly within 1000 load cycles (i.e. 75–90% of the final values) and the specimens experienced an active zone. For specimens tested at relatively lower frequencies (i.e. $f \leqslant 10$ Hz), the plastic strain was most probably influenced by particle reorientation. Some grinding or attrition of asperities occurred, but it was not expected to contribute very much to the plastic deformation; however, as f increased to 20 Hz, the active zone became more pronounced and the axial strain rate attained a maximum value. This may be attributed to the breakage of angular corners or projections (Fig. 3(a)) as well as particle reorientation. Following this active zone, the permanent deformation rate declined to an insignificant value with N, while the corresponding ε_a stabilised to a relatively steady value that was defined as the plastic shakedown zone. However, unlike ε_a, the volumetric strain ε_v continued to develop as N increased, as shown in Fig. 2(b). For a given value of σ_3', ε_v became more compressive with an increasing f.

Range II: plastic shakedown and ratcheting (30 Hz $\leqslant f \leqslant$ 50 Hz). As shown in Fig. 2(c), the triaxial specimens were initially unstable and reached plastic shakedown within 2000 load cycles, but in this plastic shakedown zone, the specimens attained an optimum packing arrangement. Larger particles were unable to slide very much, which meant the specimen produced a resilient vibration that resulted in a stable deformation. The smaller particles located in the void between the larger ones could experience high-frequency vibration. This result could induce a high degree of attrition of asperities for the larger and smaller particles, as shown in Fig. 3(b). Once this kind of corner degradation has developed to a certain extent, the larger particles will begin to slide again. Moreover, after 20 000–100 000 load cycles, the fatigue failure of particles commences and some particle splitting takes place through planes of weakness such as microcracks and other flaws (Fig. 3(c)). Both these mechanisms could contribute to any further deformation with a constant rate that is defined as the ratcheting zone. Fig. 2(d) indicates that the increase of ε_v in the ratcheting zone was more apparent than the corresponding smaller increase of ε_a.

Range III: plastic collapse ($f = 60$ Hz). Figure 2(e) shows that at extremely high frequencies, each load application resulted in a progressive increment of ε_a, such that the specimen reached the displacement limit of the actuator (at 30% axial strain) and failure occurred within 1000 load cycles. This is defined as plastic collapse. With insufficient lateral confinement ($\sigma_3' \leqslant 30$ kPa), the specimen may have had poorly established contacts and relatively small particle-to-particle contact areas, so at such high frequency (i.e. $f = 60$ Hz), the coordination number is greatly reduced, which could induce self-similar particle splitting (Fig. 3(d)), and allow relatively large-scale particle reorientation and an unstable aggregate skeleton to occur. This is in agreement with the study by McDowell *et al.* (1996), which elucidates the rapid development of permanent ε_a. For frequencies below 20 Hz (or $V = 145$ km/h), plastic shakedown was observed. For higher frequency (i.e. $f \geqslant 30$ Hz), ratcheting or plastic collapse occurs. Therefore, a speed from about 145 km/h to 220 km/h is identified as the critical train speed above which track failure may occur.

Suiker *et al.* (2005) and Lackenby *et al.* (2007) used the cyclic stress ratio $q_{max,cyc}/q_{peak,sta}$ to characterise the behaviour of ballast under cyclic loading. $q_{peak,sta}$ is the peak deviator stress at failure and can be obtained from static tests (Indraratna *et al.*, 2014b). However, Fig. 2 shows that three different deformation mechanisms exist with a unique cyclic stress ratio (i.e. $q_{max,cyc}/q_{peak,sta} = 0{\cdot}613$) while varying f from 5 Hz to 60 Hz. Hence, the $q_{max,cyc}/q_{peak,sta}$ appeared unable to capture the cyclic behaviour observed in this study. When the effect of frequency on ballast deformation is considered, it is useful to compare the cyclic cumulative axial strain $\varepsilon_{a,cyc}$, with the strain $\varepsilon_{a,sta}$ obtained from a

Table 1. Summary of cyclic triaxial tests

Test name	σ_3': kPa	$q_{max,cyc}$: kPa	f: Hz	N
C1	30	230	5	500 000
C2			10	500 000
C3			20	500 000
C4			30	500 000
C5			40	500 000
C6*			50	200 100
C7*			60	580

* $\varepsilon_a > 30\%$ before 500 000 cycles

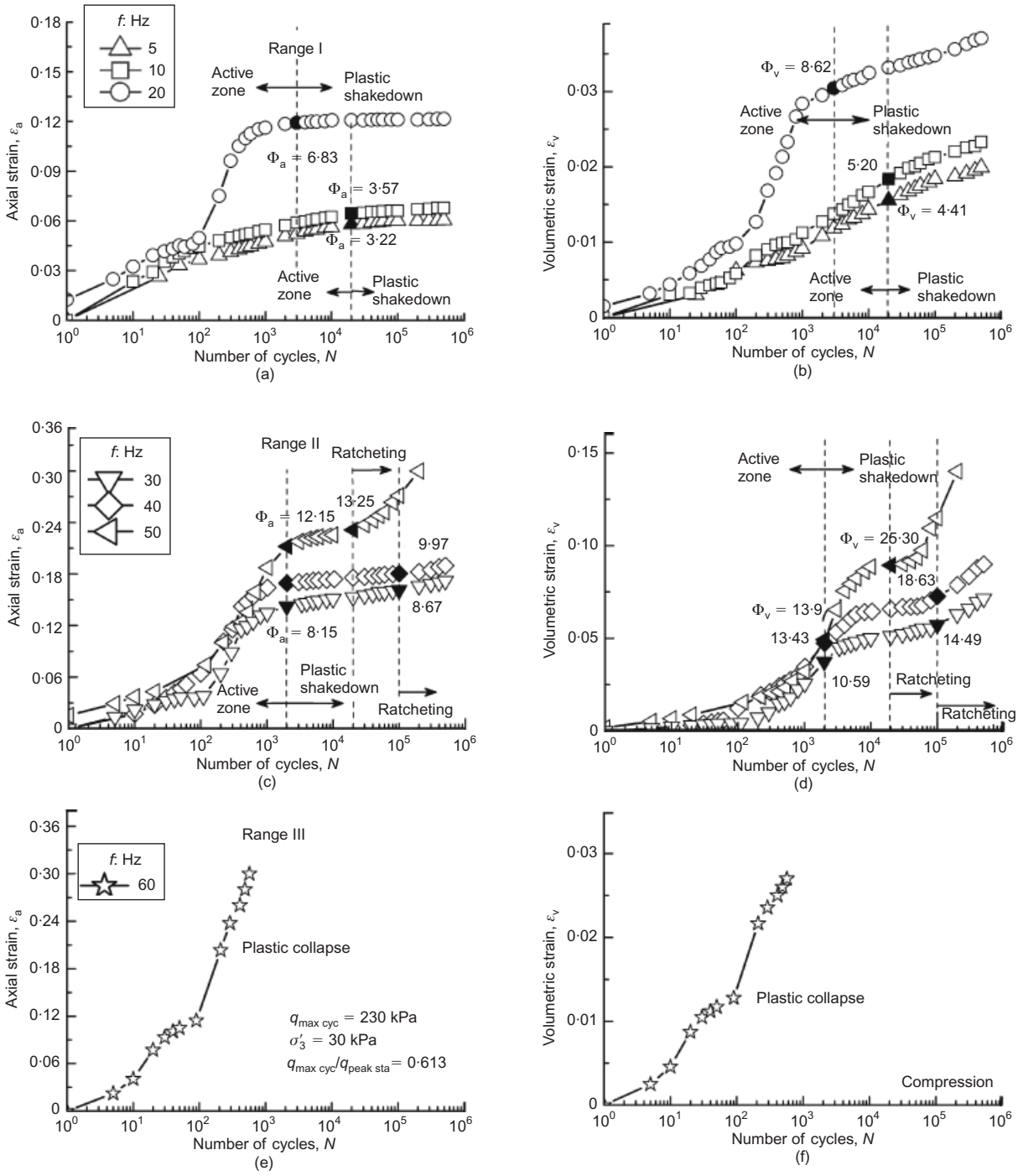

Fig. 2. Permanent strain of ballast under cyclic loading: (a, b) range I – plastic shakedown, (c, d) range II – plastic shakedown and ratcheting, and (e, f) range III – plastic collapse

monotonic test at the corresponding static load $q_{sta} = q_{max,cyc}$. The cyclic axial strain ratio (CASR), $\Phi_a = \varepsilon_{a,cyc}/\varepsilon_{a,sta}$ is therefore defined for this purpose. The values of $\varepsilon_{a,cyc}$ at the characteristic N (i.e. $N = 20\,000$ and $500\,000$) were used to calculate the CASR. Fig. 4 shows the calculated Φ_a as a function of f, and when $f \leqslant 20$ Hz, the difference between the values of Φ_a at $N = 20\,000$ and $500\,000$ was insignificant. This implies that for these specimens the shakedown phase was continued to the end of the test. However, this difference becomes visible when $f \geqslant 30$ Hz, which is because the ratcheting zone was reached after a relatively long shakedown zone as shown in Fig. 2(c). A best-fit equation for the data shown in Fig. 4 can be represented as

$$\Phi_a = ae^{bf} \tag{1}$$

where a and b are the empirical coefficients.

By considering a and b as a function of N (Fig. 4), equation (1) can be extended to capture the permanent deformation under different loading numbers and frequency while the previous study (i.e. Indraratna *et al.*, 2010a) could not capture this effect. Accumulated ε_a can be obtained as

$$\varepsilon_a = a\ \exp(0{\cdot}138bV)\varepsilon_{a,sta} \tag{2}$$

Like CASR, an empirical relation could be obtained to relate cyclic volumetric strain ratio (CVSR), Φ_v, with f (i.e. $\Phi_v = ce^{df}$). Fig. 4 shows that Φ_v was bigger than Φ_a at given values of f and N, which indicates that frequency had more influence on ε_v than ε_a.

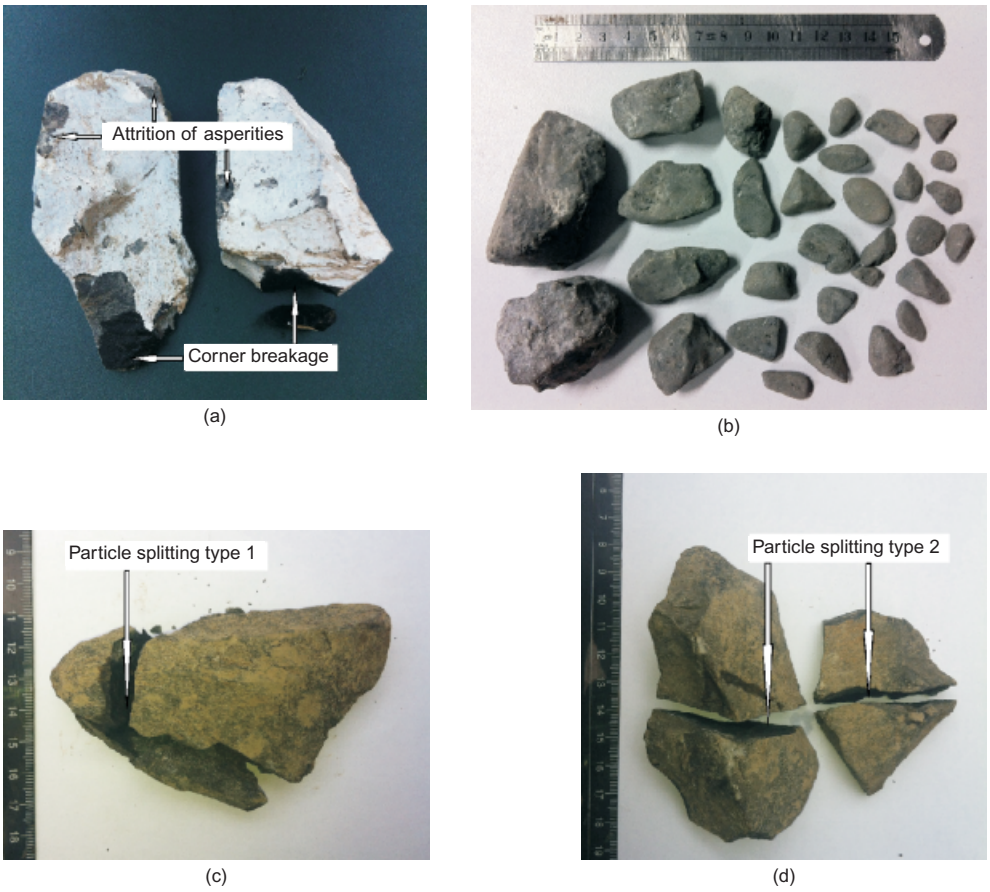

Fig. 3. Examples of particle degradation: (a) attrition of asperities and corner breakage in range I; (b) high degree attrition of asperities in range II; (c) particle splitting type 1 in range II; (d) particle splitting type 2 in range III

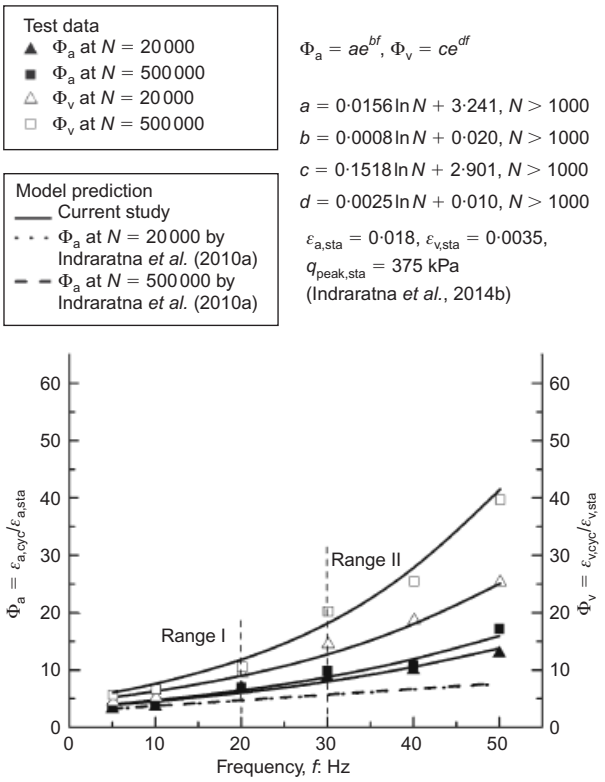

Fig. 4. Cyclic axial strain ratio and cyclic volumetric strain ratio as a function of frequency, f (data sourced from Indraratna *et al.* (2010a, 2014b))

Degradation behaviour

Figure 5(a) illustrates the relationship between the particle breakage index BBI and ε_v as a function of f at the end of test (i.e. $N = 500\,000$). As expected, the load frequency had a profound influence on the magnitude of BBI, which increased with f. For range I (i.e. $f \leqslant 20$ Hz), particle degradation was in the form of attrition of asperities and corner breakage, but for range II where the frequency was higher (i.e. $f \geqslant 30$ Hz), particle splitting caused by fatigue and a high degree of attrition became predominant, which contributed to a continual increase of volumetric deformation at a constant rate (i.e. ratcheting zone in Fig. 2(c)). In this zone there was a reasonable correlation between ε_v and BBI. The data from Fig. 5(a) are re-plotted in Fig. 5(b) as BBI against ε_v, irrespective of f. The ε_v can be related to BBI by a linear relationship defined as

$$\varepsilon_v = m\text{BBI} - n \tag{3}$$

where m and n are the empirical constants.

CONCLUSIONS

The cyclic traixal tests conducted in the present study could help to understand the long-term response of a railway track under different train speeds. The following conclusions could be drawn.

(*a*) Three different deformation mechanisms exist according to frequency (or train speed, V), namely: range I – plastic shakedown at $f \leqslant 20$ Hz (or $V \leqslant 145$ km/h), range II – plastic shakedown and ratcheting at 30 Hz $\leqslant f \leqslant$ 50 Hz

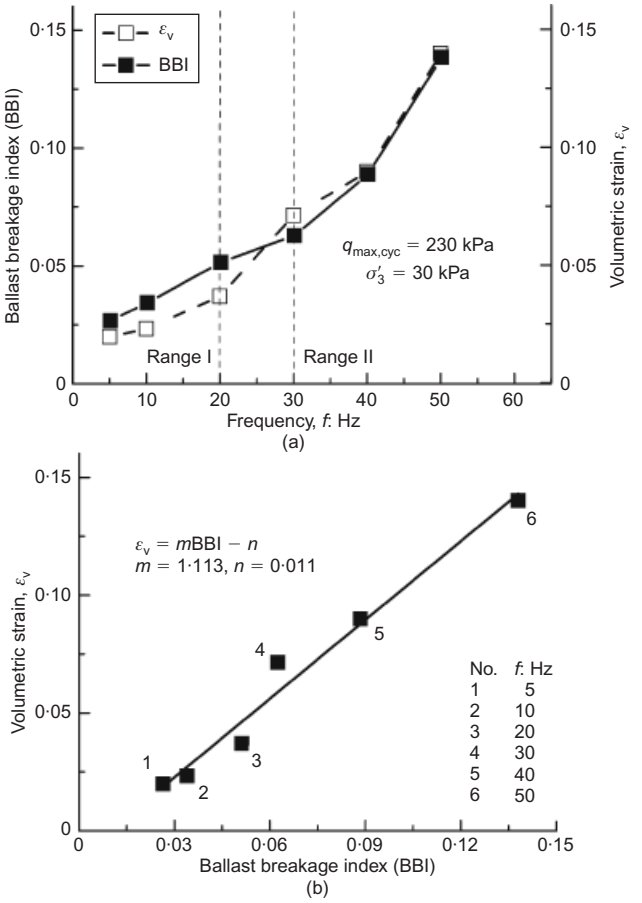

Fig. 5. Breakage and volumetric strain behaviour at the end of the tests ($N = 500\,000$): (a) as a function of frequency f, and (b) relationship between ε_v and BBI

(or 220 km/h $\leqslant V \leqslant$ 360 km/h), and range III – plastic collapse at $f \geqslant 60$ Hz (or $V \geqslant 400$ km/h).

(*b*) Cyclic axial strain ratio $\Phi_a = \varepsilon_{a,cyc}/\varepsilon_{a,sta}$ was defined to study how frequency affected the axial strain. A simple relationship for latite basalt relating Φ_a and f can be given: $\Phi_a = ae^{bf}$. A similar relationship exists between the cyclic volumetric strain ratio (Φ_v) and f: $\Phi_v = ce^{df}$. Moreover, an empirical equation was proposed to calculate ε_a: $\varepsilon_a = a \exp(0{\cdot}138bV)\, \varepsilon_{a,sta}$.

(*c*) The volumetric strain ε_v reached at the end of the tests can be related to BBI by a linear relationship that is given by: $\varepsilon_v = 1{\cdot}113\ \text{BBI} - 0{\cdot}011$.

(*d*) A critical train speed between 145 km/h and 220 km/h exists, above which track failure may occur (in the form of ratcheting or plastic collapse). This train speed should be avoided in a ballasted track or further lateral confinement may be needed in order to reduce settlement. However, this aspect needs to be analysed further and is not within the scope of current study.

ACKNOWLEDGEMENTS

This work has been financially supported by the China Scholarship Council: this support is gratefully acknowledged. The authors would like to thank Alan Grant and Ritchie McLean at University of Wollongong for their assistance in the laboratory.

NOTATION

a, b, c, d, m, n	regression coefficients
BBI	particle breakage index
C_u	coefficient of uniformity
d_{max}	maximum particle size
d_{min}	minimum particle size
d_{50}	median particle size
e_0	initial void ratio
f	cyclic loading frequency
N	number of load cycles
p'	mean effective stress
q	deviator stress
$q_{max,cyc}$	maximum deviator stress magnitude
$q_{min,cyc}$	minimum deviator stress magnitude
$q_{peak,sta}$	peak deviator stress at failure
q_{sta}	static deviator stress
V	train speed
ε_a, $\varepsilon_{a,cyc}$	cyclic axial strain
$\varepsilon_{a,sta}$	static axial strain
ε_v, $\varepsilon_{v,cyc}$	cyclic volumetric strain
$\varepsilon_{v,sta}$	static volumetric strain
σ'_3	confining pressure
Φ_a, Φ_v	cyclic axial and volumetric strain ratio, respectively

REFERENCES

Alonso-Marroquín, F., García-Rojo, R. & Herrmann, H. J. (2004). Micro-mechanical investigation of the granular ratcheting. *Proceedings of international conference on cyclic behaviour of soils and liquefaction phenomena*, Bochum, Germany, pp. 3–10. Leiden, the Netherlands: Balkema.

Banimahd, M., Woodward, P., Kennedy, J. & Medero, G. (2013). Three-dimensional modelling of high speed ballasted railway tracks. *Proc. Instn Civ. Engrs – Transport* **166**, No. 2, 113–123.

Eisenmann, J., Leykauf, G. & Mattner, L. (1994). Recent development in German railway track design. *Proc. Instn Civ. Engrs – Transport* **105**, No. 2, 91–96.

Indraratna, B., Ionescu, D. & Christie, H. D. (1998). Shear behaviour of railway ballast on large-scale triaxial tests. *J. Geotech. Geoenviron. Engng ASCE* **124**, No. 5, 439–449.

Indraratna, B., Lackenby, J. & Christie, D. (2005). Effect of confining pressure on the degradation of ballast under cyclic loading. *Géotechnique* **55**, No. 4, 325–328, http://dx.doi.org/10.1680/geot.2005.55.4.325.

Indraratna, B., Thakur, P. K. & Vinod, J. S. (2010a). Experimental and numerical study of railway ballast behaviour under cyclic loading. *Int. J. Geomech.* **10**, No. 4, 136–144.

Indraratna, B., Nimbalkar, S., Christie, D., Rujikiatkamjorn, C. & Vinod, J. S. (2010b). Field assessment of the performance of a ballasted rail track with and without geosynthetics. *J. Geotech. Geoenviron. Engng ASCE* **136**, No. 7, 907–917.

Indraratna, B., Nimbalkar, S. & Rujikiatkamjorn, C. (2014a). Enhancement of rail track performance through utilisation of geosynthetic inclusions. *Geotech. Engng J. SEAGS and AGSSEA* **45**, No. 1, 17–27.

Indraratna, B., Sun, Q. D. & Nimbalkar, S. (2014b). Observed and predicted behaviour of rail ballast under monotonic loading capturing particle breakage. *Can. Geotech. J.* http://dx.doi.org/10.1139/cgj-2013-0361.

Indraratna, B., Nimbalkar, S. & Rujikiatkamjorn, C. (2014c). From theory to practice in track geomechanics – Australian perspective for synthetic inclusions. *Transport Geotech*. http://dx.doi.org/10.016/j.trgeo.2014.07.004.

Karg, C. & Haegeman, W. (2009). Elasto-plastic long-term behaviour of granular soils: experimental investigation. *Soil Dynam. Earthquake Engng* **29**, No. 1, 155–172.

Kempfert, H. G. & Hu, Y. (1999). Measured dynamic loading of railway underground. *Proceedings of the 11th pan-American conference on soil mechanics and geotechnical engineering*, Foz do Iguacu, Brazil, pp. 843–847.

Lackenby, J., Indraratna, B., McDowell, G. & Christie, D. (2007). Effect of confining pressure on ballast degradation and deformation under cyclic triaxial loading. *Géotechnique* **57**, No. 6, 527–536, http://dx.doi.org/10.1680/geot.2007.57.6.527.

Luo, Y., Yin, H. & Hua, C. (1996). Dynamic response of railway ballast to the action of trains moving at different speeds. *Proc. IMechE, Part F: J. Rail and Rapid Transit* **210**, No. 2, 95–101.

McDowell, G. R., Bolton, M. D. & Robertson, D. (1996). The

fractal crushing of granular materials. *J. Mech. Phys. Solids* **44**, No. 12, 2079–2102.

Sloan, S. W., Krabbenhøft, K. & Lyamin, A. V. (2008). Lower bound shakedown analysis in geotechnics. *Proceedings of the 12th international conference of the International Association for Computer Methods and Advances in Geomechanics (IACMAG)*, Goa, India, pp. 328–335.

Suiker, A. S. J. & de Borst, R. (2003). A numerical model for the cyclic deterioration of railway tracks. *Int. J. Numer. Methods Engng* **57**, No. 4, 441–470.

Suiker, A. S. J., Selig, E. T. & Frenkel, R. (2005). Static and cyclic triaxial testing of ballast and subballast. *J. Geotech. Geoenviron. Engng ASCE* **131**, No. 6, 771–782.

Wichtmann, T., Niemunis, A. & Triantafyllidis, T. (2005). Strain accumulation in sand due to cyclic loading: drained triaxial tests. *Soil Dynam. Earthquake Engng* **25**, No. 12, 967–979.

Youd, T. L. (1972). Compaction of sands by repeated shear straining. *J. Soil Mech. Found. Div. ASCE* **98**, No. SM7, 709–734.